Modelling Retinal Ganglion Cells Stimulated with Static Natural Images

Gautham P. Das, Philip J. Vance, Dermot Kerr, Sonya A. Coleman
School of Computing and Intelligent Systems
Ulster University (Magee)
Londonderry, Northern Ireland, United Kingdom
Email: {g.das, p.vance, d.kerr, sa.colemen}@ulster.ac.uk

Thomas M. McGinnity
School of Science and Technology
Nottingham Trent University
Nottingham, United Kingdom
Email: martin.mcginnity@ntu.ac.uk

***Abstract*—A standard approach to model retinal ganglion cells uses reverse correlation to construct a linear-nonlinear model using a cascade of a linear filter and a static nonlinearity. A major constraint with this technique is the need to use a radially symmetric stimulus, such as Gaussian white noise. Natural visual stimuli are required to generate a more realistic ganglion-cell model. However, natural visual stimuli significantly differ from white noise stimuli and are not radially symmetric. Therefore a more sophisticated modelling approach than the linear-nonlinear method is required for modelling ganglion cells stimulated with natural images. Machine learning algorithms have proved very capable in modelling complex non-linear systems in other scientific domains. In this paper, we report on the development of computational models, using different machine learning regression algorithms, that model retinal ganglion cells stimulated with natural images in order to predict the number of spikes elicited. Neuronal recordings obtained from electro-physiological experiments in which isolated salamander retinas are stimulated with static natural images are used to develop these models. In order to compare the performance of the machine learning models, a linear-nonlinear model was also developed from separate experiments using Gaussian white noise stimuli. A comparison of the spike prediction using the models developed shows that the machine learning models perform better than the linear-nonlinear approach.**

Keywords–Retinal ganglion cells; Natural image stimulus; Linear-nonlinear models; Machine learning models.

I. INTRODUCTION

It is well established that retinal ganglion cells (RGCs) play an important role in early stage biological visual processing by generating action potentials onto the optic nerve, based on the visual stimulus that falls on the photo-receptors. Various studies have identified different types of ganglion cells present in the mammalian retina and much of their functionalities [1]–[3]. An important step towards developing artificial vision is to develop computational models of the RGCs in a biological vision system that accurately replicate biological processing.

The standard approach to model RGCs is to use a linear-nonlinear (LN) technique, which cascades a linear filter module and a static nonlinear transformation module [4]. The main advantage in using the LN technique with a single linear filter is its ease of obtaining the model parameters, particularly the shape of the linear filter [5]. However, this advantage arises from a major constraint: the retina should be stimulated with a radially symmetric stimulus, usually generated with Gaussian white noise. Although white noise stimuli are mathematically simple to analyse, it has been shown that they do not exercise the full range of neuronal behaviour and any model developed with this stimulus can emulate only a subset of responses from a biological neuron [6]. These limitations necessitate the use of natural visual stimuli to develop more realistic computational models of RGCs. Natural visual stimuli have considerably different statistical features in comparison to white noise stimuli. For example, unlike the white noise stimuli, they are not radially symmetric and have high cross-correlation between nearby pixels [6]–[8]. Therefore, a more sophisticated approach than the LN technique is required to accurately model the visual processing taking place in an RGC under natural viewing conditions.

An important characteristic observed from existing studies [9] [10] and evident in the LN technique is the nonlinear processing that takes place in an RGC. Machine learning algorithms have proven very capable in modelling complex nonlinear systems in other domains [11] [12]. In this paper, we report on the development of computational models, obtained using machine learning based regression algorithms, of RGCs stimulated with static natural images in order to predict the number of spikes elicited. In total, we explored 10 different machine learning approaches. Among these, the extreme learning machine (ELM), Bayesian regularised neural network (BRNN), support vector regression (SVR) and k-nearest neighbour (kNN) regression approaches performed better than others and their results are presented. Neuronal recordings from electro-physiological experiments, in which isolated salamander retinas are stimulated using static natural images, are used to train these models. In order to compare the performance of these machine learning models, LN models of the RGCs were also developed. In these LN models, the linear filters were estimated from the neuronal recordings from a separate experiment with Gaussian white noise stimuli and the static nonlinearities were then fitted with the recordings from the experiments with static natural image stimuli. Additional modelling experiments were performed to investigate whether adding more statistical features as inputs to the computational models can improve the prediction.

The remainder of this paper is organised as follows. Section II discusses existing studies related to the topic presented in this paper. Details of the electro-physiological experimental setup and various data pre-processing stages are discussed in Section III. Results from the modelling experiments are presented in Section IV. Section V concludes the paper and explores possible future research directions.

 ISBN: 978-1-61208-462-6

II. Related Works

System identification techniques, such as the Wiener theory [13] and Wiener-Volterra method [14] were used in earlier studies to develop computational models of visual processing in the retina. Owing to the increased computational complexities of these approaches with higher order kernels [15], the nonlinear auto-regressive moving average with exogenous inputs (NARMAX), a parametric system identification technique, has been used to model components of biological vision systems in more recent studies [16][17]. Modular models in the form of cascaded or parallel configurations have been used extensively to overcome limitations of the Volterra-Wiener models. Although different configurations of the modular models, such as linear-nonlinear (LN) [4], nonlinear-linear (NL) [18] and linear-nonlinear-linear (LNL) [19] exist, the LN technique with a single linear filter module has been widely used, due to the ease of obtaining the model parameters. An alternative to the system identification and modular methods is to use a machine learning based nonparametric regression algorithm to model the nonlinear visual processing taking place in the biological visual systems. Although multi-layer feed-forward neural networks have been used to model neurons in the visual cortex [20], few studies have explored their performance in comparison to the standard modelling techniques. This is one of the aspects addressed in this paper.

Many of the existing studies involving modelling of RGCs primarily focus on stimulation using white noise visual stimulus [5][21]. While white noise and other random patterned (e.g., moving gratings) visual stimuli enable the cell type to be distinguished (e.g., ON-cells, OFF-cells, ON-OFF cells, etc.) [22] and also specific functionalities (e.g., approaching motion detection cell, lateral motion detection cell, directionally sensitive cell, etc.) [23], they do not test the full range of neuronal behaviour [6]. It has been shown that natural images are more effective in stimulating complex cells in the primary visual cortex, while evoking low spike time variability, than when using artificial random stimuli [6][15][24]. This could be because our vision systems may have been evolutionarily adapted to the natural visual stimuli; furthermore natural image stimuli have considerably different statistical features in comparison to the artificial visual stimuli. For example, natural scenes have high spatial correlation, and their intensity distribution has considerable skewness and kurtosis [7][8], which could have substantial influence on a visual neuron's response. However, only a limited number of existing studies [18] have modelled the visual processing of natural images by RGCs. Thus, the study presented in this paper focuses specifically on developing computational models of RGCs stimulated with natural images. The influence of different statistical features of the stimuli on the neuronal responses has also been evaluated, i.e., how the computational model inputs are selected in order to improve their prediction results.

III. Electro-physiological Experimental Setup

A. Experimental Setup

Neuronal recordings were obtained from retinas of dark-adapted adult axolotl salamander (Ambystoma mexicanum) using in vitro electro-physiological experiments [25]. The retina was isolated and placed with the ganglion-cell-side down on a planar multi-electrode array for extracellular recordings. To visually stimulate the retina, the screen of a gamma-corrected miniature organic light-emitting diode (OLED) monitor was focussed onto the photoreceptor layer of the retina. The stimulus screen was updated with a frame rate of 60Hz. Action potentials were recorded from the RGCs using the multi-electrode array, and were sampled at a frequency of 10kHz.

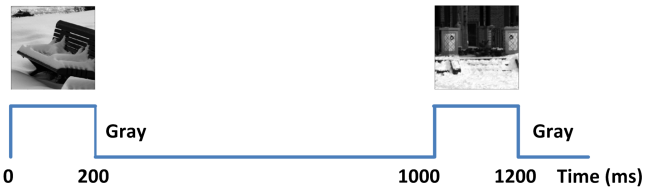

Figure 1. Stimulus updates during experiments with natural image stimuli. In each trial, an image was shown for 200ms followed by gray screen to recover from any adaptation to the natural image.

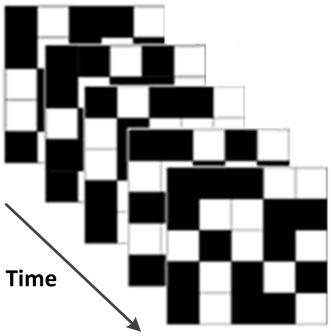

Figure 2. Binary checker board flicker. Each stimulus pattern is shown for 33.33ms.

Each trial with a natural image involved the stimulation of the retina for 1000ms, in which the natural image was displayed for 200ms followed by a full-field gray image for 800ms (see Figure 1). The full-field gray image helps the ganglion cells to recover from any adaptation to the natural image. In total, 300 natural images were used to stimulate the retina and each image was repeated in 13 such trials to observe the variations in the spiking behaviours. The spikes recorded within a time period of 300ms from the onset of the natural image to 100ms after the image is replaced with the gray screen, allowing for the processing delay of the RGC, is considered to be in response to the natural image.

In order to obtain the linear filter parameters for the LN models, neural responses were recorded from the retina when stimulated with a binary checker-board flicker stimulus (a spatio-temporal artificial stimulus, Figure 2). The stimulus update rate in this experiment was different from that used for the natural images experiments. The stimulus was updated at a rate of 30Hz, meaning a new stimulus pattern was presented approximately every 33.33ms. The recorded spikes for this stimulus were binned at the stimulus rate, i.e., a bin corresponds to a time period of 33.33ms. Data from this experiment consisted of 64500 samples of stimulus and corresponding binned spike recordings for a timespan of nearly 36 minutes.

B. Stimulus Pre-processing

Both visual stimuli (natural images and checker-board flickers) used to stimulate the retina vary spatially in light

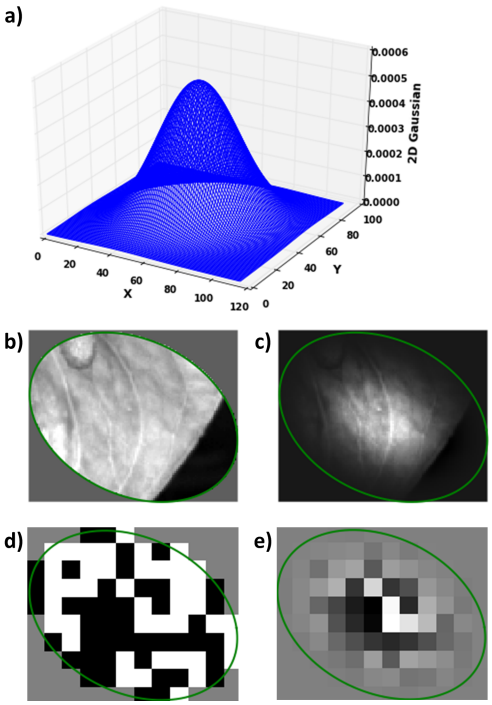

Figure 3. Stimulus pre-processing for Cell-14: (a) 2D Gaussian weighting used, (b) Local stimulus (natural image), (c) Gaussian weighted local stimulus (natural image), (d) Local stimulus (checker-board flicker) and (e) Gaussian weighted local stimulus (checker-board flicker).

intensity. Depending on the spatial arrangement of a pixel (of the visual stimulus) in the receptive field (RF) region of an RGC, the effect of light intensity on the RGCs spiking behaviour differs. This is usually a maximum at the centre and reduces gradually as it moves towards the periphery of the RF region. In order to emulate this, the local stimulus (the area of the visual stimulus that falls within the RF region) of each RGC is weighted using a 2D Gaussian filter (with a support of 3σ). Two examples, one each for the natural image stimulus and the checker-board flicker stimulus, showing the Gaussian weighting are presented in Figure 3.

IV. Modelling Experiments

Computational models were developed to predict the rate of spikes generated by the RGCs for each natural image stimulus. The mean response from 13 repeated trials (spikes per trial) is selected as the target spike rate for training the computational models. The selection of input parameters to the computational models is discussed in Section IV-A. Details of the modelling techniques used for developing the computational models are briefly discussed in Section IV-B and the results from the modelling experiments are discussed in Section IV-C.

A. Selection of Inputs to the Models

Natural images have considerably different statistical features in comparison with artificial visual stimuli, which are generally used to stimulate the retina in electro-physiological experiments. From the Gaussian weighted local stimulus different statistical features, namely the mean, standard deviation, skewness and kurtosis, were extracted and their correlation with the neuronal response was analysed to identify the input parameters to the models. Only those RGCs with the 3σ RF region falling within the image boundary and having

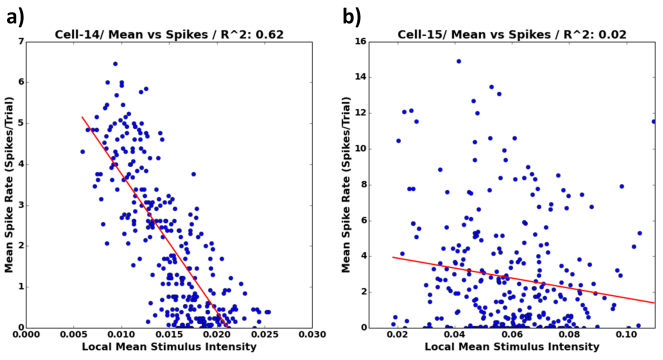

Figure 4. Correlation between local mean stimulus intensity and mean spike rate (spikes/trial): (a) for Cell-14 with good correlation and (b) for Cell-15 with poor correlation. R^2 values are also given as a measure of correlation. The red line represents the best linear fit for the points.

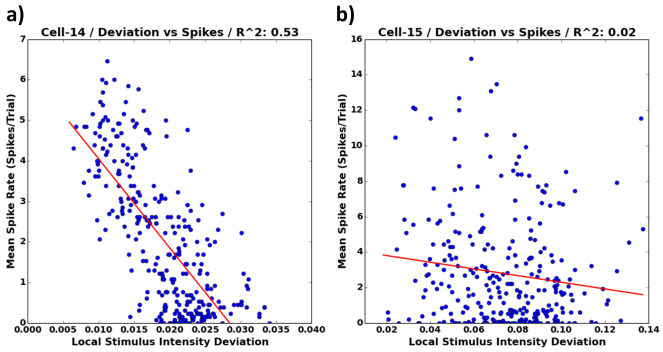

Figure 5. Correlation between local stimulus intensity deviation and mean spike rate (spikes/trial): (a) for Cell-14 with good correlation and (b) for Cell-15 with poor correlation. R^2 values are also given as a measure of correlation. The red line represents the best linear fit for the points.

elicited spikes for a majority of the images were selected for modelling. A general consensus among existing studies on the modelling of RGCs is that the spiking behaviour correlates with the mean intensity or mean contrast. In our analysis, the majority of the RGCs had substantial correlation between mean intensity and neuronal spiking, while others had very poor correlation. An example is shown in Figure 4 for two randomly selected sample cells, Cell-14 with good correlation (Figure 4(a)) and Cell-15 with poor correlation (Figure 4(b)).

Among the cells with good correlation between the mean intensity and the spike rate, the local stimulus intensity deviation also had good correlation with the spike rate. This is shown in Figure 5 for Cell-14 and Cell-15. It was found that the skewness and kurtosis, although quite different from that observed in random artificial stimuli, had little correlation with the neuronal spiking. The scatter plots showing this are presented in Figure 6.

From this analysis, only the mean and standard deviation of local stimulus intensity were identified to be important in predicting the cell's response. Only those cells that showed good correlation between the local mean stimulus intensity and the spike rate were selected for modelling. Two sets of computational models were developed to check whether including more input parameters would improve the overall prediction performance. The first set was developed with the local mean stimulus intensity as the only input parameter to the models. The second set was developed with the local mean stimulus intensity and the local stimulus intensity deviation as the input parameters to the models.

 ISBN: 978-1-61208-462-6

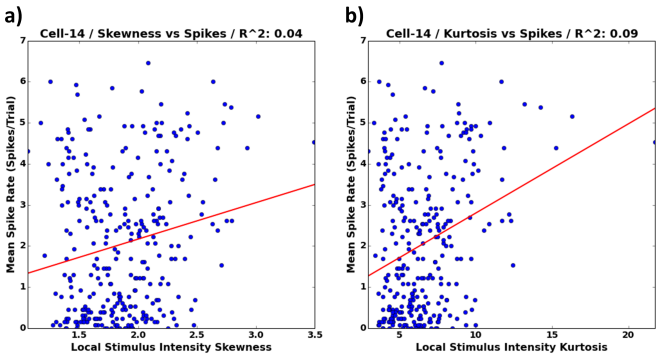

Figure 6. Correlation between and mean spike rate (spikes/trial) and (a) local stimulus intensity skewness, and (b) local stimulus intensity kurtosis and mean spike rate (spikes/trial). The red line represents the best linear fir for the points.

B. Modelling Techniques

The LN technique [5] to model an RGC separates the model into a linear filter and a nonlinear function, which are cascaded to estimate the spike rate corresponding to each visual stimulus. The LN technique used here involves only one linear filter, although multiple filters are possible [26]. The shape of the linear filter is approximated by the spike triggered average (STA) stimulus for the neuronal recording using the Gaussian white noise checker-board flicker stimulus. The STA is defined as the average stimulus preceding a spike in the cell. This can be mathematically represented as:

$$STA = \frac{\sum_{t=1}^{T} \overrightarrow{s_t(\tau)} f_t}{\sum_{t=1}^{T} f_t} \quad (1)$$

where T is the total time period in which spikes were recorded, $\overrightarrow{s_t(\tau)}$ is the sequence of mean stimulus intensity (mean of the Gaussian weighted local stimulus intensity, Figure 3(e)) from time $(t-\tau)$ to time t, and f_t is the number of spikes recorded at time t. In this work, the value of τ was identified as 21 time bins. The static nonlinearity is represented by a parameterised form of a cumulative normal density function [5]. In order to fit this nonlinearity, the target spike rate was approximated by the total number of spikes in a time bin.

The LN models were developed with only the local mean stimulus intensity as input. Although not addressed here, two options to include more than one input parameter are to have the same number of linear filters as the number of input parameters, and to combine the input parameters linearly or nonlinearly to form a single parameter.

Machine learning based regression algorithms used here include ELM, BRNN, SVR and kNN regression. The ELM [27] is based on single hidden layer feed-forward networks. The back-propagation technique used for training in feed-forward neural networks is replaced in the ELMs by random assignment of weights of the hidden layer neurons and analytical assignment of weights of the output layer neurons to speed up the training process. The BRNN [28] is a feed-forward neural network, which incorporates Bayesian regularisation into the training process to reduce potential overfitting and overtraining which commonly occur in the back-propagation technique. The SVR [29] is an extension of the popular support vector machine (SVM) classifier to regression problems. In this, a complex nonlinear relationship

TABLE I. MAXIMUM MEAN SPIKE RATE OF THE SELECTED RGCS

Cell-ID	*Spike Rate*	*Cell-ID*	*Spike Rate*	*Cell-ID*	*Spike Rate*
Cell-07	10.231	Cell-31	13.462	Cell-39	13.615
Cell-14	6.462	Cell-32	9.615	Cell-42	5.923
Cell-16	8.308	Cell-33	14.692	Cell-47	17.538
Cell-23	14.000	Cell-34	13.615		

in the original space is transformed to a linear relationship in a higher-dimensional feature space. In the kNN regression algorithm [30], the value corresponding to an input is predicted as the average of its closest k neighbours from the training samples in a feature space. The parameters of the machine learning models were estimated using five-fold cross validation with five repeats.

C. Results

Among the 300 natural images, neuronal recordings for 150 images were selected for training the models, while the neuronal recordings for the remaining 150 images were used for testing. In order to compare the performance of these models three metrics, namely root mean square error (RMSE), coefficient of determination (R^2) and Kendall's rank correlation coefficient (Tau) between the actual spike counts observed in the electro-physiological experiments and the model predictions, are used. Smaller values of RMSE, and larger values of R^2 and Tau are desired. Modelling results from 11 different RGCs are presented here. The maximum spike rate from these RGCs are given in Table I, while they all had a minimum spike rate of zero.

The first set of models was developed with the local mean stimulus intensity as the only input using the LN, ELM, BRNN, SVR and kNN techniques. Performances of these models for the test samples are compared using the three metrics – RMSE in Table II, R^2 in Table III and Kendall's Tau in Table IV. In general, it can be seen that the machine learning models performed better than the LN technique in terms of RMSE and R^2, while the LN technique performed better in terms of Kendall's Tau for majority of the RGCs. From these results, although the improvement in the performances is marginal, it can be observed that the machine learning algorithms provide a good alternative to the standard LN technique in modelling RGCs stimulated with natural images.

The second set of models was developed with the mean and standard deviation of the local stimulus intensity as the input parameters. As the LN technique used in this work has only one linear filter, the mean and standard deviations could not be used simultaneously as inputs. As the machine learning algorithms performed on par or marginally better for the first set of models, only these approaches were used to develop the second set of models. Performances of these models for the test samples of the same RGCs are compared using the same three metrics - RMSE in Table V, R^2 in Table VI and Kendall's Tau in Table VII. A comparison between the corresponding metric comparison tables (RMSE in Tables II and V, R^2 in Tables III and VI, and Kendall's Tau in Tables IV and VII) shows that adding the local stimulus intensity deviation as an additional input has not resulted in any major improvement for majority of the modelled RGCs. This could be because of the high correlation between the mean and the standard deviation of local stimulus intensity (Figure 7). Due to this, both these inputs could be feeding in similar and thus redundant information to the models.

 ISBN: 978-1-61208-462-6

TABLE II. RMSE BETWEEN ACTUAL SPIKE RATE AND PREDICTED SPIKE RATE FROM THE FIRST SET OF MODELS. SMALLER VALUES INDICATE BETTER PERFORMANCE.

Cell-ID	*LN*	*SVR*	*ELM*	*kNN*	*BRNN*
Cell-07	1.114	1.133	1.120	1.127	**1.101**
Cell-14	1.042	1.031	1.030	1.035	**1.026**
Cell-16	1.703	1.679	1.646	1.669	**1.645**
Cell-23	2.419	2.443	2.401	**2.381**	2.396
Cell-31	**1.666**	1.801	1.853	1.772	1.724
Cell-32	1.836	2.050	**1.739**	1.871	1.900
Cell-33	2.639	2.680	3.131	2.665	**2.631**
Cell-34	2.996	2.837	**2.681**	2.824	2.684
Cell-39	**2.951**	3.241	3.035	3.084	3.030
Cell-42	1.662	1.581	**1.568**	1.595	**1.568**
Cell-47	2.956	2.981	2.950	2.961	**2.937**

TABLE III. R^2 BETWEEN ACTUAL SPIKE RATE AND PREDICTED SPIKE RATE FROM THE FIRST SET OF MODELS. LARGER VALUES INDICATE BETTER PERFORMANCE.

Cell-ID	*LN*	*SVR*	*ELM*	*kNN*	*BRNN*
Cell-07	0.778	0.771	0.773	0.769	**0.780**
Cell-14	**0.630**	0.626	0.627	0.621	**0.630**
Cell-16	0.294	**0.331**	0.324	0.294	0.325
Cell-23	**0.241**	0.225	0.220	0.237	0.222
Cell-31	**0.637**	0.587	0.543	0.578	0.601
Cell-32	0.411	**0.460**	0.456	0.371	0.343
Cell-33	**0.608**	0.576	0.506	0.570	0.588
Cell-34	0.256	0.341	**0.352**	0.282	0.349
Cell-39	0.265	**0.270**	0.262	0.206	0.260
Cell-42	0.105	**0.121**	0.117	0.100	0.117
Cell-47	**0.299**	0.287	0.282	0.279	0.286

TABLE IV. KENDALL'S TAU BETWEEN ACTUAL SPIKE RATE AND PREDICTED SPIKE RATE FROM THE FIRST SET OF MODELS. LARGER VALUES INDICATE BETTER PERFORMANCE.

Cell-ID	*LN*	*SVR*	*ELM*	*kNN*	*BRNN*
Cell-07	**0.671**	0.631	0.654	0.668	0.668
Cell-14	**0.542**	0.536	0.536	0.538	0.537
Cell-16	**0.416**	0.410	0.407	0.385	0.407
Cell-23	0.355	0.342	0.351	**0.376**	0.340
Cell-31	0.501	0.48	0.485	**0.505**	0.502
Cell-32	0.374	0.359	**0.375**	0.367	0.329
Cell-33	**0.565**	0.519	0.548	0.534	0.542
Cell-34	0.271	0.319	0.326	0.266	**0.337**
Cell-39	**0.358**	0.343	0.341	0.271	0.340
Cell-42	0.225	0.237	**0.244**	0.223	**0.244**
Cell-47	**0.397**	0.362	0.376	0.374	0.376

TABLE V. RMSE BETWEEN ACTUAL SPIKE RATE AND PREDICTED SPIKE RATE FROM THE SECOND SET OF MODELS. SMALLER VALUES INDICATE BETTER PERFORMANCE.

Cell-ID	*SVR*	*ELM*	*kNN*	*BRNN*
Cell-07	**1.109**	1.298	1.147	1.322
Cell-14	1.047	1.171	**1.024**	1.034
Cell-16	1.662	**1.625**	1.658	1.635
Cell-23	2.414	**2.368**	2.447	2.380
Cell-31	**1.678**	1.744	1.848	1.797
Cell-32	1.930	1.871	1.906	**1.865**
Cell-33	2.588	**2.452**	2.696	2.472
Cell-34	2.829	4.663	**2.769**	2.771
Cell-39	3.321	3.045	**3.043**	3.067
Cell-42	1.581	1.581	1.614	**1.579**
Cell-47	3.092	2.948	3.108	**2.921**

TABLE VI. R^2 BETWEEN ACTUAL SPIKE RATE AND PREDICTED SPIKE RATE FROM THE SECOND SET OF MODELS. LARGER VALUES INDICATE BETTER PERFORMANCE.

Cell-ID	*SVR*	*ELM*	*kNN*	*BRNN*
Cell-07	**0.774**	0.712	0.766	0.691
Cell-14	0.602	0.576	0.616	**0.623**
Cell-16	0.346	**0.370**	0.309	0.340
Cell-23	0.230	**0.235**	0.210	0.229
Cell-31	**0.638**	0.599	0.561	0.575
Cell-32	**0.389**	0.366	0.353	0.371
Cell-33	0.601	0.632	0.566	**0.634**
Cell-34	**0.315**	0.053	0.307	0.300
Cell-39	0.211	0.233	**0.242**	0.225
Cell-42	0.114	**0.122**	0.082	0.104
Cell-47	0.238	0.276	0.213	**0.293**

TABLE VII. KENDALL'S TAU BETWEEN ACTUAL SPIKE RATE AND PREDICTED SPIKE RATE FROM THE SECOND SET OF MODELS. LARGER VALUES INDICATE BETTER PERFORMANCE.

Cell-ID	*SVR*	*ELM*	*kNN*	*BRNN*
Cell-07	0.656	0.623	**0.669**	0.598
Cell-14	0.541	**0.572**	0.543	0.556
Cell-16	0.426	**0.437**	0.422	0.421
Cell-23	**0.374**	0.359	0.369	0.360
Cell-31	0.490	**0.504**	0.484	0.490
Cell-32	0.279	0.375	**0.376**	0.345
Cell-33	0.539	0.572	0.528	**0.584**
Cell-34	0.334	**0.338**	0.337	0.303
Cell-39	0.306	**0.331**	0.309	0.324
Cell-42	0.242	0.244	0.182	**0.246**
Cell-47	0.376	**0.406**	0.341	0.395

V. DISCUSSION AND FUTURE WORK

Ganglion cells are the first spiking neurons in the visual pathway, and accurately modelling them is an important step towards a refined understanding of retinal functions in natural visual environments and the development of a biologically inspired artificial vision system. Most of the existing studies that addressed this have used an artificial visual stimulus to evoke spikes from the RGCs. As the artificial visual stimuli have different statistical features and cannot generate the same range of neuronal responses in comparison with the natural image stimuli, realistic models of RGCs should be derived from neuronal responses to natural image stimuli. This has been addressed in the work presented by applying different machine learning approaches to develop computational models of RGCs, which have been stimulated with natural images. From the results it can be seen that the machine learning approaches provide a good alternative to the standard LN technique in modelling RGCs. The modelling experiments were performed in two stages. Initially the mean intensity of the local stimulus region of each RGC was selected as the input parameter to the models. Further modelling experiments used the standard deviation of the local stimulus intensity as an additional input parameter, which marginally improved the prediction results for some RGCs.

There are many future directions to this research. An obvious one is to move from static images to temporal image sequence of natural images (movies). However, further improvements could be made to the current models before that - (i) by using a better estimate of the RF region and (ii) by considering the lateral interconnections that could affect the spiking behaviour. A contributing factor towards the marginal performance improvements of the machine learning models could be the crude approximation of the RF region with 3σ support and then weighting it with the 2D Gaussian. An alternative way to estimate the RF region is given in [18]. However, further experiments are necessary to compare these two methods. The modelling experiments presented in this paper treat the neuronal spiking behaviour of each cell individually. However, this is not the case in a biological system. There are many lateral interconnections in the retina through horizontal and amacrine cells that could result in an excitatory or inhibitory effect on nearby RGCs [31] and could be more evident for a natural image stimulus. Further modelling experiments are

 ISBN: 978-1-61208-462-6

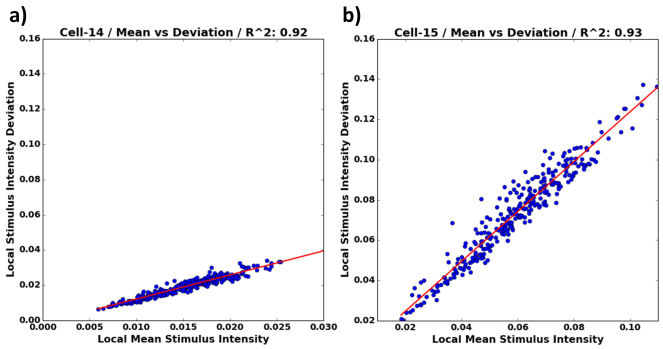

Figure 7. Correlation between local mean stimulus intensity and local stimulus intensity deviation: (a) for Cell-14 and (b) for Cell-15. R^2 values are also given as a measure of correlation. The red line represents the best linear fit for the points.

necessary to include such spatio-temporal correlations into the RGC models. Furthermore, it is difficult to identify a single machine learning approach that works for all RGCs. Depending on the type of the RGC (e.g., approach motion detection, lateral motion detection, etc.), the features in the image that stimulate the cell vary and a machine learning algorithm may perform best for a specific type of RGC. In future modelling experiments, we will also be looking into this.

ACKNOWLEDGMENT

The research leading to these results has received funding from the European Union Seventh Framework Programme [FP7-ICT-2011.9.11] under grant number [600954] ["VISUALISE"]. The experimental data contributing to this study have been supplied by the "Sensory Processing in the Retina" research group at the Department of Ophthalmology, University of Göttingen as part of the VISUALISE project.

REFERENCES

[1] R. J. Lucas, "Mammalian inner retinal photoreception," Curr. Biol., vol. 23, no. 3, 2013, pp. R125–R133.

[2] O. Marre et al., "Mapping a complete neural population in the retina," J. Neurosci., vol. 32, no. 43, 2012, pp. 14 859–14 873.

[3] R. H. Masland, "The neuronal organization of the retina," Neuron, vol. 76, no. 2, 2012, pp. 266–280.

[4] S. Ostojic and N. Brunel, "From spiking neuron models to linear-nonlinear models," PLoS Comput. Biol., vol. 7, no. 1, 2011.

[5] E. J. Chichilnisky, "A simple white noise analysis of neuronal light responses," Netw. Comput. Neural Syst., vol. 12, no. 2, 2001, pp. 199–213.

[6] V. Talebi and C. L. Baker, "Natural versus synthetic stimuli for estimating receptive field models: A comparison of predictive robustness," J. Neurosci., vol. 32, no. 5, 2012, pp. 1560–1576.

[7] R. A. Frazor and W. S. Geisler, "Local luminance and contrast in natural images," Vision Res., vol. 46, no. 10, 2006, pp. 1585–1598.

[8] E. P. Simoncelli and B. A. Olshausen, "Natural image statistics and neural representation," Annu. Rev. Neurosci., vol. 24, no. 1, 2001, pp. 1193–1216.

[9] T. Gollisch, "Features and functions of nonlinear spatial integration by retinal ganglion cells," J. Physiol., vol. 107, no. 5, 2013, pp. 338–348.

[10] M. Meister and M. J. Berry II, "The neural code of the retina," Neuron, vol. 22, no. 3, 1999, pp. 435–450.

[11] S. Bind, A. K. Tiwari, and A. K. Sahani, "A survey of machine learning based approaches for Parkinson disease prediction," Int. J. Comput. Sci. Inf. Technol., vol. 6, no. 2, 2015, pp. 1648–1655.

[12] M. Zhang, Artificial Higher Order Neural Networks for Modeling and Simulation. Hershey, PA: Information Science Reference (an imprint of IGI Global), 2013.

[13] P. Z. Marmarelis and K. I. Naka, "White-noise analysis of a neuron chain: an application of the Wiener theory," Science, vol. 175, no. 4027, 1972, pp. 1276–1278.

[14] M. J. Korenberg and I. W. Hunter, "The identification of nonlinear biological systems: Volterra kernel approaches," Ann. Biomed. Eng., vol. 24, no. 2, 1996, pp. 250–268.

[15] R. Herikstad, J. Baker, J.-P. Lachaux, C. M. Gray, and S.-C. Yen, "Natural movies evoke spike trains with low spike time variability in cat primary visual cortex," J. Neurosci., vol. 31, no. 44, 2011, pp. 15 844–15 860.

[16] D. Kerr, M. McGinnity, and S. Coleman, "Modelling and analysis of retinal ganglion cells through system identification," in Proc. Int. Conf. Neural Comput. Theory Appl., 2014, pp. 158–164.

[17] Z. Song et al., "Biophysical modeling of a drosophila photoreceptor," in Proc. Int. Conf. Neural Inf. Process. Part I, C. S. Leung, M. Lee, and J. H. Chan, Eds., vol. 5863. Springer-Verlag Berlin Heidelberg, 2009, pp. 57–71.

[18] X. Cao, "Encoding of natural images by retinal ganglion cells," PhD Thesis, University of Southern California, 2010.

[19] M. J. Korenberg, H. M. Sakai, and K. Naka, "Dissection of the neuron network in the catfish inner retina: III. Interpretation of spike kernels," J. Neurophysiol., vol. 61, 1989, pp. 1110–1120.

[20] R. Prenger, M. C.-K. Wu, S. V. David, and J. L. Gallant, "Nonlinear V1 responses to natural scenes revealed by neural network analysis," Neural Networks, vol. 17, no. 5-6, 2004, pp. 663–679.

[21] H. M. Sakai, K. Naka, and M. J. Korenberg, "White-noise analysis in visual neuroscience," Vis. Neurosci., vol. 1, no. 3, 1988, pp. 287–296.

[22] H. K. Hartline, "The response of single optic nerve fibers of the vertebrate eye to illumination of the retina," Am. J. Physiol., vol. 121, 1938, pp. 400–415.

[23] T. Gollisch and M. Meister, "Eye smarter than scientists believed: Neural computations in circuits of the retina," Neuron, vol. 65, no. 2, 2010, pp. 150–164.

[24] J. Touryan, G. Felsen, and Y. Dan, "Spatial structure of complex cell receptive fields measured with natural images," Neuron, vol. 45, no. 5, 2005, pp. 781–791.

[25] J. K. Liu and T. Gollisch, "Spike-triggered covariance analysis reveals phenomenological diversity of contrast adaptation in the retina," PLOS Comput. Biol., vol. 11, no. 7, 2015, p. e1004425.

[26] T. Gollisch and M. Meister, "Modeling convergent on and off pathways in the early visual system," Biol. Cybern., vol. 99, no. 4-5, 2008, pp. 263–278.

[27] E. Cambria et al., "Extreme learning machines," IEEE Intell. Syst., vol. 28, no. 6, 2013, pp. 30–59.

[28] F. D. Forsee and M. T. Hagan, "Gauss-Newton approximation to Bayesian learning," in Proc. 1997 IEEE Int. Conf. Neural Networks, 1997, pp. 1930–1935.

[29] C. Cortes and V. Vapnik, "Support-vector networks," Mach. Learn., vol. 20, no. 3, 1995, pp. 273–297.

[30] N. S. Altman, "An introduction to kernel and nearest-neighbor nonparametric regression," Am. Stat., vol. 46, no. 3, 1992, pp. 175–185.

[31] J. W. Pillow et al., "Spatio-temporal correlations and visual signalling in a complete neuronal population." Nature, vol. 454, no. 7207, 2008, pp. 995–999.

 ISBN: 978-1-61208-462-6